Weierstraß-Institut
für Angewandte Analysis und Stochastik

im Forschungsverbund Berlin e.V.

Preprint ISSN 0946 – 8633

Contact-line instability of dewetting thin films

Andreas Münch[§], Barbara Wagner[1] [1]

submitted: Apr. 26, 2004

[1] Weierstrass Institute for Applied Analysis and Stochastics,
Mohrenstrasse 39, 10117 Berlin, Germany
[§] Institute of Mathematics, Humboldt University, 10099 Berlin, Germany

No. 924
Berlin 2004

1991 *Mathematics Subject Classification.* 74D10,74F05,74F10,77N25.

Key words and phrases. Lubrication approximation, stability, slippage.

Edited by
Weierstraß-Institut für Angewandte Analysis und Stochastik (WIAS)
Mohrenstraße 39
10117 Berlin
Germany

Fax: + 49 30 2044975
E-Mail: preprint@wias-berlin.de
World Wide Web: http://www.wias-berlin.de/

Abstract

We investigate the linear stability of dewetting thin polymer films on hydrophobised substrates driven by Van-der-Waals forces, using a lubrication model. We focus on the role of slippage in the emerging instability at the three-phase contact-line and compare our results to the corresponding no-slip case. Our analysis shows that generically, small perturbations of the receding front are amplified, but in the slippage case by orders of magnitude larger than in the no-slip case. Moreover, while the perturbations become symmetrical in the no-slip case, they are asymmetrical in the slippage case. We furthermore extend our lubrication model to include effects of nonlinear curvature.

1 Introduction

A thin liquid film that wets a solid substrate is typically subject to contact-line instabilities such as formation of fingers. Such phenomena have been studied for decades, both theoretically and experimentally, for films driven by forces such as gravity [9, 31, 1, 32], or Marangoni stresses or both [6, 5, 7, 11, 2]. The derivation of the mathematical models exploits the separation of length scales to obtain a simplified lubrication model from the underlying Navier-Stokes equations in conjunction with conservation of mass. The stress singularity at the three phase contact-line, which is inherited by the resulting 4th order PDE, is regularized for example via a slip boundary condition or precursor model, where the height of the precursor or the slip length is usually much smaller than the height of the actual wetting film. Interestingly, for the wetting phenomena just mentioned, the choice of the boundary condition at the three phase contact-line enters only weakly in that it does not influence the eventual appearance of fingers, see for example [1, 11, 13, 17]. In contrast to these wetting phenomena, contact-line instabilities for dewetting thin films have received only limited attention particularly theoretically.

For such a process to occur, a thin, viscous film is uniformly spread onto a hydrophobic surface. It then dewets in a process that is initiated either spontaneously through spinodal decomposition or induced for example through nucleation. The dry spots, or holes, that form as a result subsequently grow as the newly formed contact line recedes, thereby accumulating liquid in a characteristic capillary ridge at the edge of the hole, which increases in width and height as the dewetting proceeds. In a variety of experimental situations it is observed that, while in some cases, the growth of the hole continues until it collides with neighboring holes, in other cases the ridge of the hole destabilizes into finger-like structures eventually pinching off and forming

droplets, see [12, 22, 25, 28, 29, 33, 16, 19]. Because of the impact this has on the emerging macroscopic pattern, it is important to understand the dynamics leading to such an instability.

Let us note here, that in contrast to the wetting scenarios the film thickness in dewetting experiments is typically by orders of magnitude smaller. For such situations, the relevance of slippage at the liquid/solid interface for the instability has been discussed by several authors, [30, 24, 14], but detailed theoretical investigations using a fluid mechanical model to understand the effect of slippage have not yet been carried out. In [20, 3, 10] the dewetting rate and shape of the ridge has been treated using approximate formulas derived from scaling arguments and energy balances. This has been compared to dewetting rates and shapes by numerically solving the corresponding lubrication model, both for the no-slip and slippage case, see [8, 15]. In [15] also the case for very hydrophobic substrates is investigated. For such situations contact angles are typically quite large and violate the small slope assumption of lubrication theory, suggesting to include the full nonlinear expression for the curvature of the liquid surface.

In this paper we study the linear stability of the dewetting ridges, by perturbing about the solutions found in [15]. In section 2, we describe the relevant physical situation and derive the lubrication model. In section 3 we discuss the two asymptotic cases: the no-slip case and the free slippage case for the lubrication model as well as for the extended model that includes nonlinear curvature. Subsequently, we detail the numerical methods used and present our results. In section 4, we summarize our results.

2 Formulation

2.1 Effective interface potential

The physical situation that underlies our mathematical model consists of a thin viscous polymer film using polystyrene (PS) of low molecular weight ($\sim$ 5kg/mol) and about 100–200 nm thick, that is uniformly spread on a substrate, consisting essentially of a silicon wafer (Si) covered with silicon oxide (SiO) layer, which is in turn covered with a monolayer of octadecyl-trichlorosilane (OTS). For such a multilayer system, it could be shown in [27], [26], how to reconstruct a corresponding effective interface potential. This can then be used to characterize the stability properties of the thin film with respect to spinodal decomposition and nucleation with the aim to extract information for the resulting dewetting pattern.

The effective interface potential is composed of repulsive and attractive long-range Van der Waals contributions, with a separate contribution for each of the layers of the substrate, and a short-range term which accounts for Born-type repulsion. The latter term provides a cut-off by penalizing a thinning of the film below a positive thickness threshold given by the minimum h_* of the potential. This is illustrated in

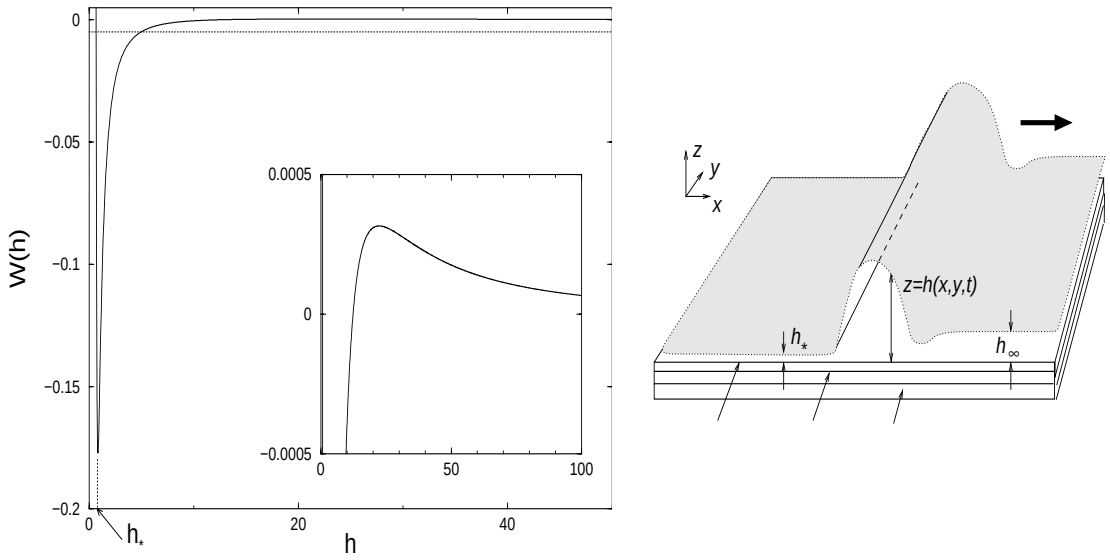

Figure 1: Left: The non-dimensional effective interface potential $W(h)$, as given by (7), with a minimum at h_* and a maximum as shown in the inset. The inset corresponds to the area above the thin dotted line in the main figure. Right: Sketch of a portion of a dewetting polymer film of initial thickness h_∞. The dewetting front and the ridge propagate in the direction of the positive x-axis, as indicated by the bold-face arrow, leaving behind a residual film of thickness h_*.

figure 1, depicting $W(h)$, which also shows correspondingly a portion of a ridge as it dewets in the x-direction from a straight front oriented in y-direction. We let d_{SiO} be the thickness of the SiO layer and d_{OTS} the thickness of the monolayer of OTS. The effective potential for this situation is (see [27]):

$$W(h) = \frac{c_{\mathrm{s}}}{h^8} - \frac{A_{\mathrm{OTS}}}{12\pi h^2} + \frac{A_{\mathrm{OTS}} - A_{\mathrm{SiO}}}{12\pi(h + d_{\mathrm{OTS}})^2} + \frac{A_{\mathrm{SiO}} - A_{\mathrm{Si}}}{12\pi(h + d_{\mathrm{OTS}} + d_{\mathrm{SiO}})^2}. \tag{1}$$

where c_{s} denotes the strength of the short-range part of the potential, and A_{SiO}, A_{Si} and A_{OTS} are the Hamaker constants of PS on SiO, Si and OTS respectively. We note that the actual values of the constants A_{OTS} and A_{SiO} turn out to nearly cancel out, so we can neglect the third term in what follows. For this system, it has been observed experimentally, that after formation of holes and formation of a ridge at the dewetting fronts of the holes, the ridges destabilize into finger-type structures.

2.2 Lubrication model

In order to describe the evolution of the film surface $z = h(x, y, t)$ we use a lubrication model that includes the influence of surface tension and the effective interface potential W of the air/OTS/PS/SiO/Si layer. In this case the pressure at $z = h(x, y, t)$ is given by

$$p = \sigma \Delta h - W''(h). \tag{2}$$

Making use of the small length scale of h one can then derive the lubrication model from the Navier-Stokes equation in conjunction with conservation of mass. In dimensional form, the lubrication model is

$$3\eta\frac{\partial h}{\partial t} + \nabla\left[m(h)\left(\sigma\nabla\Delta h - W''(h)\nabla h\right)\right] = 0, \tag{3}$$

where η and σ are the liquid viscosity and the liquid surface tension, respectively, and $W''(h)$ is the second derivative of the effective interface potential with respect to the PS film thickness h. As a first approximation for the short chained (2-5kg/mol) variants of PS, which has an entanglement length of $\sim$18kg/mol, our lubrication model (3) treats the polymer film in its melt state as a Newtonian liquid, so that in particular viscoelastic effects are not present in the model.

Also, $m(h)$ is a non-negative mobility coefficient, the form of which depends on the boundary conditions at the liquid/solid interface. A widely used condition relates the slippage velocity v of the liquid at the wall to the local shear rate $\partial v/\partial z$ via

$$v = \beta\,\partial v/\partial z, \tag{4}$$

where the slip length β is defined as the distance below the interface at which the liquid velocity extrapolates to zero. Usually, the slip length is very small, on the order of ten to a few hundred nanometers for Newtonian liquids and it only becomes relevant in the immediate vicinity of the contact line, or when considering very thin films as we do here. For the above slip boundary condition at the substrate, the mobility has the form $m(h) = h^3 + \beta h^2$ with a non-zero slip length. The no-slip boundary condition is obtained if $\beta = 0$, so that the mobility has the form $m(h) = h^3$. On the other hand, the limit $\beta \to \infty$ yields the mobility $m(h) = h^2$, after rescaling time with β.

Finally, we non-dimensionalize our problem by minimizing the number of parameters that appear in the equation. We require the time derivative of h, the contribution from surface tension and the first terms in $W''(h)\nabla h$ to balance. This is achieved with the following choices

$$H = \left(\frac{144\pi c_{\mathrm{s}}}{A_{\mathrm{SiO}}}\right)^{\frac{1}{6}},\ L = 4\pi\left(\frac{81\sigma^3 {c_{\mathrm{s}}}^2}{2\pi {A_{\mathrm{SiO}}}^5}\right)^{\frac{1}{6}},\ T = \frac{288\pi^3\eta\sigma}{{A_{\mathrm{SiO}}}^3}\left(\frac{324 {c_{\mathrm{s}}}^5 A_{\mathrm{SiO}}}{\pi}\right)^{\frac{1}{6}} \tag{5}$$

for the normal and parallel length scales and for the time scale. Introducing these scalings for h, x, y and for t we obtain

$$\frac{\partial h}{\partial t} + \nabla\left[m(h)\left(\nabla\Delta h - \left\{\frac{1}{h^{10}} - \frac{1}{h^4} + \frac{a}{(h+d)^4}\right\}\nabla h\right)\right] = 0. \tag{6}$$

Note that in (6) the slip length β, which is contained in the mobility $m(h)$, has also been scaled with H. The expression in curly brackets is the second derivative of the following non-dimensional form of the effective interface potential,

$$W(h) = \frac{1}{72h^8} - \frac{1}{6h^2} + \frac{a}{6(h+d)^2}, \tag{7}$$

which contains two parameters, namely

$$a = (A_{\mathrm{SiO}} - A_{\mathrm{Si}})/A_{\mathrm{SiO}} \qquad \text{and} \qquad d = (d_{\mathrm{OTS}} + d_{\mathrm{SiO}})/H. \tag{8}$$

2.3 Nonlinear curvature

The OTS layer used in the experiments is very hydrophobic towards PS so that this system produces a contact angle of almost 60^o, see [27]. This leads us to also consider nonlinear curvature, replacing the linearized expression in (6). This means, for comparison, we also investigate the model

$$\frac{\partial h}{\partial t} + \nabla \left[m(h) \left(\nabla \kappa - W^{''}(h) \nabla h \right) \right] = 0, \tag{9}$$

where

$$\kappa(x,y,t) = \frac{\left(1+\rho^2 h_y^2\right) h_{xx} - 2\rho^2 h_x h_y h_{xy} + \left(1+\rho^2 h_x^2\right) h_{yy}}{\left(1+\rho^2\left(h_x^2+h_y^2\right)\right)^{3/2}}, \tag{10}$$

with

$$\rho = \frac{H}{L} = \frac{1}{2}\left(\frac{{A_{\mathrm{SiO}}}^4}{18\pi^4\sigma^3 c_s}\right)^{1/2}, \tag{11}$$

reducing to the linearized curvature for $\rho \to 0$. For easy reference, we will refer to (9), (10) as the 'nonlinear curvature model', while we continue to use the term 'lubrication model' for (6).

3 Linear stability of the dewetting thin film

3.1 Non-constant base states

The stability analysis of a dewetting ridge we consider here, is to some degree non-standard in that the base state about which we perturb is, in several ways, non-constant, so that the usual travelling wave ansatz or similarity ansatz with a priori known exponents is not appropriate. Here, the dewetting ridge (see figure 1) accumulates liquid as it moves to the right. As a consequence, the height as well as width of the ridge increases. Furthermore, the velocity of the receding ridge is non-constant and changes as the ridge evolves; the spreading law depends on the boundary condition at the liquid/solid interface, which means it is different for the two mobilities considered in this paper.

In a similar setting like ours, [20] used energy balances to predict dewetting rates that are independent of the size of the receding ridge if no-slip boundary conditions are used at the contact-line, thus the ridge would move at a constant velocity.

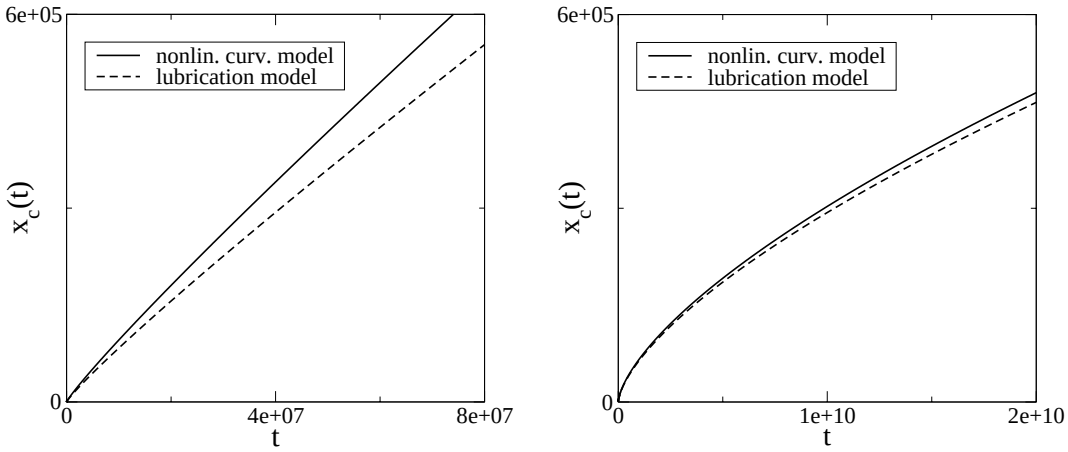

Figure 2: Evolution of the contact line position with time for the no-slip (a) and the slip case (b).

This result was corrected to a somewhat lower than linear dewetting law in [8] by numerical integration of the corresponding lubrication model. In [15] it was found that an ansatz with a logarithmic correction could be excellently fit to the numerical solution found by integrating the one dimensional version of the lubrication and the nonlinear curvature model in one space dimension,

$$\frac{\partial h}{\partial t} + \frac{\partial}{\partial x}\left[m(h)\left(\frac{\partial}{\partial x}\left(\frac{h_{xx}}{(1+\rho^2 h_x^2)^{3/2}}\right) - W^{''}(h)\nabla h\right)\right] = 0. \tag{12}$$

for $m(h) = h^3$ (letting $\rho = 0$ to recover the lubrication model). Note that by using this one-dimensional model we consider here the evolution of trenches rather than of axisymmetric holes. The fit was in any case much better than with an ansatz assuming a linear time dependence for $x_c(t)$. Here $x_c(t)$ denotes the position of the front, and is taken to be the inflection point on the 'dry' side of the ridge, i.e. the side facing the region from which the liquid film has receded. A plot of the numerical solution is shown in fig. 2(a), showing two curves for the nonlinear curvature and the lubrication model that are both close, but still visibly different, from a straight line.

For the free slip case, when $m(h) = h^2$, [21, 23] predict a $t^{2/3}$-law for the evolution of the dewetting front, which reads in scaled form using (5)

$$x_c(t) = \frac{3^{2/3} C^{1/3}}{4^{2/3}} \frac{\theta_s^{5/3}}{h_\infty^{1/3}}\, t^{2/3}, \qquad C \approx 0.1, \tag{13}$$

where θ_s is the static contact angle. By fitting a power-law ansatz, [15] finds that (13) indeed compares well with the numerical solution of (12) with mobility $m(h) = h^2$. The numerical solutions for the nonlinear curvature model and the lubrication model ($\rho = 0$) are both shown in fig. 2(b).

For the computations in fig. 2 and all other computations presented below, we used

the physical parameters given in [18]:

$$c_s = 4 \cdot 10^{-81}\,\mathrm{J m^6}, \quad A_{\mathrm{OTS}} = 2.2 \cdot 10^{-20}\,\mathrm{J}, \quad A_{\mathrm{Si}} = -1.4 \cdot 10^{-19}\,\mathrm{J}, \qquad (14)$$
$$d_{\mathrm{OTS}} + d_{\mathrm{Sio}} = 4.4 \cdot 10^{-9}\,\mathrm{m}, \quad \sigma = 30.8 \cdot 10^{-3}\,\mathrm{N m^{-1}}.$$

This leads to the following scalings:

$$H = 2.085 \cdot 10^{-10}\,\mathrm{m}, \qquad L = 1.290 \cdot 10^{-10}\,\mathrm{m}.$$

The viscosity and hence the time scale varies greatly for different chain lengths, moreover, it depends strongly on the temperature. Below we present our results for the stability analysis as a function of the dewetting front position, which does not require the knowledge of the time scale.

Note that the length scales are very small (in the sub-nanometric range) which is to be expected since the balance we used to fix them includes the Born repulsion term in the potential which acts only over very small scales. As a result, the residual film h_* will be an order one value in the scaled variables, while the size of the ridge or the distance it travels will be orders of magnitude larger. The values of the non-dimensional parameters in the potential are

$$a = 7.36, \quad d = 21.1.$$

Then, the minimum of the potential W is $h_* = 0.833$ (equivalent to 0.174 nm). The initial profile and in particular the initial thickness of the wetting film are the same as in section 3.3.

3.2 The linearized problem

As next step we describe the occurrence of fingers in the ridge, in terms of the evolution of a small perturbation $h_{\mathrm{b}}(x,t)$. We introduce the perturbation

$$h(x,y,t) = h_{\mathrm{b}}(x,t) + \delta h_1(x,t)\exp(iqy)$$

into the lubrication model, with $\delta \ll 1$ and retain only linear terms in δ. The curvature κ can then be written as

$$\kappa(x,y,t) = \kappa_{\mathrm{b}}(x,t) + \delta\,\kappa_1(x,y,t)$$

where

$$\kappa_{\mathrm{b}}(x,t) = \frac{h_{\mathrm{b}xx}}{(1+\rho^2 h_{\mathrm{b}x}^2)^{3/2}} \qquad (15)$$

and

$$\kappa_1(x,y,t) = \frac{h_{1xx} + ((1+\rho^2 h_{\mathrm{b}x}^2))\; h_{1yy}}{(1+\rho^2 h_{\mathrm{b}x}^2)^{3/2}} - \frac{3\rho^2 h_{\mathrm{b}x} h_{\mathrm{b}xx}}{(1+\rho^2 h_{\mathrm{b}x}^2)^{5/2}} h_{1x}. \qquad (16)$$

We obtain for the linearized equation

$$\frac{\partial h_1}{\partial t} + \mathcal{L}h_1 + \frac{\partial}{\partial x}\left[m(h_\mathrm{b})\frac{\partial}{\partial x}\left(\frac{h_{1yy}}{(1+\rho^2 h_{\mathrm{b}x}^2)^{1/2}}\right)\right] + \frac{m(h_\mathrm{b})}{(1+\rho^2 h_{\mathrm{b}x}^2)^{1/2}}\frac{\partial^4 h_1}{\partial y^4} \tag{17}$$
$$+m(h_\mathrm{b})\frac{\partial^2}{\partial y^2}\left(\frac{h_{1xx}}{(1+\rho^2 h_{\mathrm{b}x}^2)^{3/2}} - \frac{3\rho^2 h_{\mathrm{b}x}h_{\mathrm{b}xx}}{(1+\rho^2 h_{\mathrm{b}x}^2)^{5/2}}h_{1x} - W^{''}(h_\mathrm{b})\,h_1\right) = 0,$$

where

$$\mathcal{L}h_1 = \frac{\partial}{\partial x}\left[m^{'}(h_\mathrm{b})\left(\kappa_{\mathrm{b}x} - W^{''}(h_\mathrm{b})\,h_{\mathrm{b}x}\right)h_1 - m(h_\mathrm{b})W^{'''}(h_\mathrm{b})\,h_{\mathrm{b}x}h_1\right. \tag{18}$$
$$\left.+m(h_\mathrm{b})\left(\frac{\partial}{\partial x}\left[\frac{h_{1xx}}{(1+\rho^2 h_{\mathrm{b}x}^2)^{3/2}} - \frac{3\rho^2 h_{\mathrm{b}x}h_{\mathrm{b}xx}}{(1+\rho^2 h_{\mathrm{b}x}^2)^{5/2}}h_{1x}\right] - W^{''}(h_\mathrm{b})\,h_{1x}\right)\right]$$

We remark that by letting $\rho = 0$ in (17), (18) and in the base state equations (9), we recover the system describing the linearization for the lubrication model.

Next we Fourier-transform (17), (18) with respect to y, which results in a system of spatially one-dimensional PDEs that depends on the span-wise wavenumber k. Note that since the coefficients of the linearized PDE are now non-constant, the solutions for the linearized problem cannot be obtained via a classical eigenvalue approach. Instead, we solve the initial value problems obtained from the linearisation numerically for a fixed set of wavenumbers, in tandem with the equation for the base state, and observe how the perturbations evolve in time. Both the equation for the base state (12) and the equation for the perturbation (17) coupled to it were discretized using a finite-difference scheme with implicit time discretisation, in some cases using the scheme proposed by [34]; this was also our approach for the linear curvature model.

3.3 Results of the linear stability analysis

The profile employed as initial condition for the base state is a steep front connecting the dewetted region, where the film thickness is h_*, and the unperturbed film of thickness h_∞, so that $\lim_{x\to-\infty} h = h_*$ and $\lim_{x\to\infty} h = h_\infty$. The initial front, specifically, its inflection point, is located at the origin. For the numerical experiments here, we usually set h_∞ to a reference value, $h_{\mathrm{ref}} = 20.8$ (noting in passing that this is $25h_*$). Recall that h_* is the film thickness that corresponds to the minimum of the potential (7) and is energetically strongly preferred compared to the initial thickness, so that in the computations the film dewets i.e. the front moves to the right.

An initial perturbation $h(t)$ is introduced at a certain time t_0, defined below, using the following expression:

$$h_1(x,t_0) = \frac{\partial h_b}{\partial x}(x,t_0), \tag{19}$$

which corresponds to a 'zig-zag' perturbation, i.e. for a non-zero wave-number, we perturb both sides of the ridge in the same direction [4]. For zero wave-number,

(19) simply represents an infinitesimal initial shift of the whole profile. Below, we also make some remarks on other choices of the initial data for h_1.

To describe the growth of bumps and eventually fingers in the ridges, we employ the amplification *A(t)* of the perturbation with respect to the initial state,

$$A(t) = \frac{\max_x |h_1(x,t)|}{\max_x |h_1(x,t_0)|} \qquad \text{for} \quad t_0 \leq t \leq t_1.$$

We compare amplifications achieved for the no-slip and the slip case at the same position of the dewetting fronts, rather than at the same value of t.

The evolution of the ridge profile happens on quite different time scales for the no-slip and the slip case, as can be expected, since the mobilities for the no-slip and the slip case differ by a factor of $h^3/h^2 = h$, which is typically on the order of, or larger than h_∞, in the ridge and the 'wetted' area. Therefore, we present the results the our stability analysis in terms of the position $x_c(t)$ of the dewetting front, rather than in terms of the dimensionless time t itself. In particular, we introduce the perturbation (19) in each of the four cases studied here (no-slip/slip, lubrication/nonlinear curvature model) when $x_c(t)$ has reached a fixed position $=$ 26.7. This leads to four different values for t_0, one for each case. Then, the evolution of the base state and the perturbation coupled to it are followed until $x_c(t_1) = 4.5 \cdot 10^5$, which again specifies a different value for t_1 in each of the cases.

From a heuristic point of view, the fact that the front evolves like $x_c(t) \sim t^\lambda$ with $\lambda < 1$, hence slows down as it grows, indicates that thicker, wider ridges move slower than thinner ones. This has been suggested as a mechanism for the instability (see e.g. [24]): Starting with some initial undulation of the ridge, thicker regions will tend to stay behind compared to the more rapidly dewetting thinner regions, thus reinforcing the differences and giving rise to a pattern of protruding bumps or fingers separated by straight portions or troughs. We expect the effect to be more pronounced for smaller λ, i.e. for the slip case, and weaker for λ equal or close to one, i.e. for the no-slip case.

We now present the results for the linear stability analysis. Figure 3 displays $A(t)$ vs. the front position $x_c(t)$ for several wavelengths $l = 2\pi/q$, for the no-slip and the slip case, and for both the lubrication and the nonlinear curvature model. In all these cases and for each of the depicted wavelengths, the perturbation grows as the dewetting proceeds, then it reaches a maximum, after which it decays. Longer wavelengths achieve the maximal amplification factor

$$A_{\max} := \max_{t \geq t_0} A(t)$$

at later stages of the dewetting, when the front has advanced further into the film and the ridge of the base state has grown in size, suggesting that the most amplified wavelength correlates with the width of the ridge [14]. This coincides interestingly with results on the fingering in gravity and Marangoni-driven flows, where the most amplified wavelength in the modal analysis is proportional to the length scale imposed by the bump width [32], and with predictions for the breaking up of static ridges [4] into droplets.

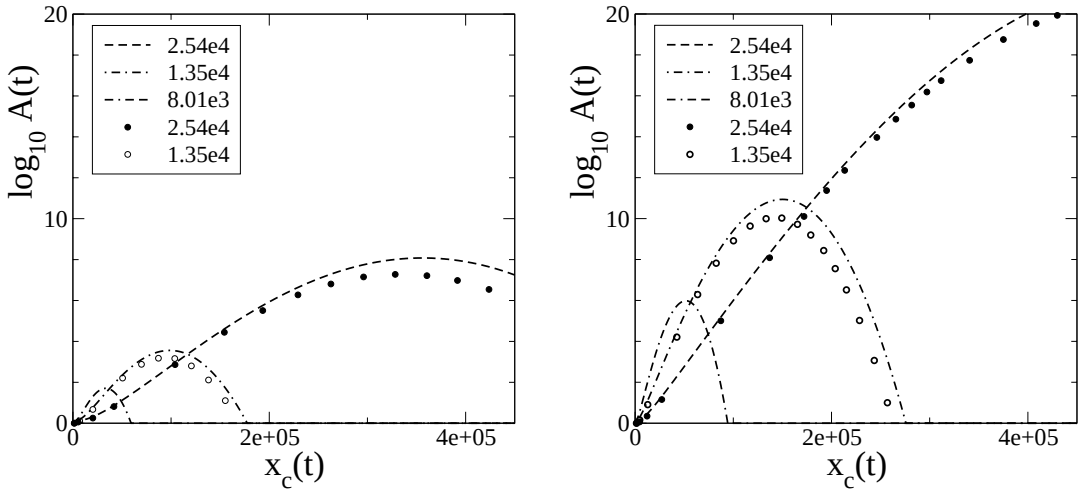

Figure 3: Amplification $A(t)$ of the perturbation versus front position $x_c(t)$ (a) for the no-slip ($m = h^3$) and (b) for the slip case ($m = h^2$). Line styles correspond to different span-wise wavelengths as indicated in the legend, and represent the results for the model using nonlinear curvature. For the model with linear curvature, we include the curves for two wavelengths, using open and solid circles

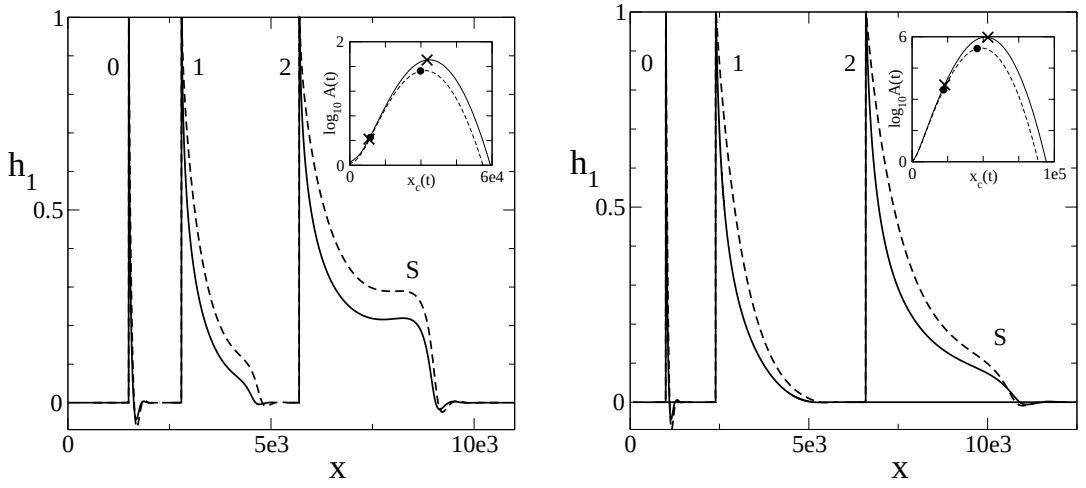

Figure 4: Perturbation profiles h_1 for wave length $l = 8.01 \cdot 10^3$, for the no-slip case (a) and the slip case (b) at different positions x_c of the front in the base profile. The profiles for h_1 have been normalized so that their maximum is one, and shifted along the x-axis, for easier comparison. For each subfigure, the perturbation profiles are labelled 0, 1 and 2, where label 0 denotes the initial perturbation introduced at t_0. Label 1 and 2 correspond to the front position/amplification factor given by the left and right cross (or circle) in the inset, respectively. Solid lines and crosses are used for the results for the nonlinear curvature model, while dashed lines and circles represent the results for the linear curvature model.

Comparing now the no-slip and the slip situation, we find that for a given wavelength, the maximum $A_{\max}$ is achieved earlier in the no-slip case, i.e. at a smaller value of x_c. More importantly, the value of $A_{\max}$ is lower, by up to several orders of magnitude, than for the slip scenario. This suggests that with slippage, the dewetting front is orders of magnitude more susceptible to span-wise perturbations of the front. We also compare, with slip and with no-slip, the amplification factors for the lubrication and the nonlinear curvature model, shown in fig. 3. The amplification factor for the latter seem to be slightly larger, but this difference is small and becomes apparent only when the growth is about to saturate.

Figure 4 shows profiles of the perturbation h_1 at different stages of amplification for both the no-slip (a) and the slip case (b) and highlights a characteristic property. In the no-slip case, the initial perturbation (given by (19)), which has one pronounced maximum and a minimum, rapidly evolves into a new profile where the minimum is replaced by a 'bump' which becomes a second maximum when $A(t)$ reaches its maximum value $A_{\max}$. This means that both the front and the back side of the ridge are perturbed, in such a way that at locations where the 'dry' side of the ridge is shifted to lower x, the 'wet' side is shifted to larger x and vice-versa. Such a perturbed ridge will consist of a sequence of thicker and thinner portions reminiscent of a varicose or 'peristaltic' mode leading to the breakup of static ridges [4].

Conversely, for the slip case, the minimum fades out much more slowly and even for the perturbation profile at maximum amplification $A(t) = A_{\max}$, we only have a small 'bump' in the position where the no-slip case has a second maximum. Thus, with slippage, the perturbation hardly affects the 'wet' side of the ridge, meaning that the ridge stays relatively flat there; undulations would appear asymmetrically, i.e. mainly on the 'dry' side of the ridge. We confirmed in seperate computations (restricted to the slip case of the lubrcation model) that this asymmetric corrugation was observed for the slip case for different initial data. For each of our choices for $h_1(x, t_0)$, the perturbation profile quickly relaxed into the shapes shown in Figure 4 (b) by dashed lines.

Comparing the results for the lubrication and the nonlinear curvature model, we find that, interestingly, the positive parts of the normalized perturbation profiles for the former model lie above those for the latter. This difference is diminished, however, if we consider the effect of these perturbations on contours of the surface. This is typically what we observe when we look at experimental data from a bird's eye perspective. Also note that, for the purpose here, the contact line can be approximated by the contour line at the height $h_b(x_c(t))$ of the inflection point of the base state. We compare this to the change induced by a perturbation on the contour line at the height where the base state has a second inflection point, i.e. on the 'wet' side of the ridge.

Corrugating a contour line by a small sinusoidal perturbation $\delta\varphi(y)$, $0 < \delta \ll 1$, locally changes the profile to

$$h_b(x + \delta\varphi(y)) = h_b(x) + \delta h_{b,x}\varphi(y) \quad + \quad \text{HOT},$$

i.e., the contour corrugation $\varphi(y)$ corresponds to a perturbation $h_1(x,y) = h_{b,x}\varphi(y)$ of the profile, and vice-versa. Hence the left and right part of the perturbation profiles shown in fig. (4) has to be scaled by some measure of the slope on the 'dry' and the 'wet' side of the base state to assess the true impact on the contact line/contours. As an estimate, we take here the slopes at the inflection points. These slopes for the slip case are 0.58 and -0.22 for the 'dry' and 'wet' side of the ridge for the lubrication model, respectively, and 0.94 and -0.24 for the nonlinear curvature model. With no-slip, they are only slightly different. In order for the difference in the slopes for the lubrication and the nonlinear curvature model to account for the difference of the perturbation profiles near label 'S' in fig. 4(b), multiplying the solid line by the ratio $(v_1\, v_4)/(v_2\, v_3) = 1.5$ must approximately yield the dashed line near 'S', and indeed it does. Hereby, v_i, $i = 1, \ldots 4$ denote the values for the slopes in the order they appear in the text above. For the noslip case (fig. 4(a)), too, the difference between the perturbation profiles near label 'S' is greatly reduced upon multiplying the solid curve with the ratio of the four values, which we found to be 1.4.

Scaling the height of points of minimal slope on the two sides of the perturbation profiles with the aforementioned values greatly reduces the difference between these heights obtained for the dashed and solid lines.

4 Conclusions

We investigated the lubrication model and an extended model that includes the full nonlinear curvature, describing the dewetting process of a thin polymer film on a hydrophobized substrate. The model assumed the dewetting process is driven by Van der Waals forces and for the mobility we used either a no-slip or a free slip condition. We showed that the receding, slowly increasing ridge at the border of each trench is unstable with respect to small span-wise perturbations. Interestingly, our linear stability analysis shows that the amplification rate is by several orders of magnitude larger for the free slip case than for the no-slip case for both the lubrication model and the extended model. Moreover, by comparing the perturbation profiles $h_1(x,t)$, we found that in the no-slip case the profiles develop two maxima, one on the front side towards the trench and the other one on the back side towards the thin film, while for the free slip case only one maximum on the front side develops. The means that for the the free slip case would show asymmetric protrusions extending towards the trench, while for the no-slip case the (by orders of magnitude smaller) protrusions are symmetrical.

Finally we want to make some remarks on preliminary results regarding the wavelength of the instability. First, we adapted our code for the dynamic base state to determine, the fastest growing wavelength for a *static* ridge of height h_{ref}. The wavelength was about four times the width of the ridge measured between the two inflection points, with a slightly larger ratio for the nonlinear curvature model. This agrees with values given in [4].

To find out whether such a relation between width of ridge and preferred wavelength holds, we performed some preliminary computations for the dewetting ridge, where we divided the wavelength $l = 2\pi/q$ by the width of the ridge at which either the amplification factor or the growth rate $\dot{A}(t)$ becomes maximal, and found that the numerical values obtained for each of these ratios hardly changed for different choices of the wavenumber k. We note that we took for width of the ridge twice the distance of the front (i.e. the inflection point) from the maximum of the ridge, and restricted this part of our investigation to the slip case. For the lubrication model and wavelengths $l = 13.5 \cdot 10^3$, $l = 8.01 \cdot 10^3$ and $l = 5.00 \cdot 10^3$, the maximum amplification factor was achieved when the ratio of wavelength and width was equal to 2.5; at the time of maximal growth rate – which occured earlier – we obtained values in the range 2.75 ± 0.1. For the nonlinear curvature model, these values were only slightly larger, upto about 10%. For both models the corresponding values do not differ much if larger wavelengths are taken into consideration. This suggests that there could to be limiting values for these ratios as the wavelengths increase. For the nonlinear curvature model and shorter wavelengths the ratio of ridge width at the moment of maximum growth rate and wavelength tends to increase. We are currently investigating these trends further.

Acknowledgements

AM was supported in part by the DFG grant MU 1626/2-1 and a Heisenberg scholarship. The authors thank Chiara Neto, Karin Jacobs, Ralph Seemann, Tom Witelski, Ralph Blossey for helpful discussions.

References

[1] A. L. Bertozzi and M. P. Brenner. Linear stability and transient growth in driven contact lines. *Phys. Fluids*, 9(3):530–539, March 1997.

[2] A. L. Bertozzi, A. Münch, X. Fanton, and A. M. Cazabat. Contact line stability and 'undercompressive shocks' in driven thin film flow. *Phys. Rev. Lett.*, 81(23):5169–5172, December 1998.

[3] F. Brochard-Wyart, P.-G. de Gennes, H. Hervert, and C. Redon. Wetting and slippage of polymer melts on semi-ideal surfaces. *Langmuir*, 10:1566–1572, 1994.

[4] F. Brochard-Wyart and C. Redon. Dynamics of liquid rim instabilities. *Langmuir*, 8:2324–2329, 1992.

[5] J. B. Brzoska, F. Brochard-Wyart, and F. Rondelez. Exponential growth of fingering intabilities of spreading films under horizontal thermal gradients. *Europhysics Letters*, 19:97–102, 1992.

[6] A. M. Cazabat, F. Heslot, S. M. Troian, and P. Carles. Finger instability of this spreading films driven by temperature gradients. *Nature*, 346(6287):824–826, August 1990.

[7] N. Garnier, R. O. Grigoriev, and M. F. Schatz. Optical manipulation of microscale fluid flow. *Physical Review Letters*, 91:Art.–No. 054501, 2003.

[8] A. Ghatak, R. Khanna, and A. Sharma. Dynamics and morphology of holes in dewetting of thin films. *Journal of Colloid and Interface Science*, 212:483–494, 1999.

[9] H. Huppert. Flow and instability of a viscous current down a slope. *Nature*, 300:427–429, 1982.

[10] K. Jacobs, R. Seemann, G. Schatz, and S. Herminghaus. Growth of holes in liquid films with partial slippage. *Langmuir*, 14:4961–4963, 1998.

[11] D. E. Kataoka and S. M. Troian. A theoretical study of instabilities at the advancing front of thermally driven coating films. *Journal of Colloid and Interface Science*, 192:350–362, 1997.

[12] R. Konnur, K. Kargupta, and A. Sharma. Instability and morphology of thin liquid films on chemically heterogeneous substrates. *Physical Review Letters*, 84(5):931–934, 2000.

[13] P. G. López, S. G. Bankoff, and M. J. Miksis. Non-isothermal spreading of a thin liquid film on an inclined plane. *Journal of Fluid Mechanics*, 11:1–39, 1996.

[14] J.-L. Masson, O. Olufokunbi, and P. F. Green. Flow instabilities in entangled polymer films. *Macromolecules*, 35:6992–6996, 2002.

[15] A. Münch. Dewetting rates of thin liquid films. Submitted to *Journal of Physics: Condensed Matter*, 2004.

[16] A. Münch, C. Neto, R. Seemann, and K. Jacobs. Fingering instability in dewetting films induced by slippage. To be submitted, 2004.

[17] A. Münch and B. A. Wagner. Numerical and asymptotic results on the linear stability of a thin film spreading down a slope of small inclination. *European Journal of Applied Mathematics*, 10:297–318, 1999.

[18] C. Neto. Private Communications.

[19] C. Neto and K. Jacobs. Physica A. Submitted, 2003.

[20] C. Redon, F. Brochard-Wyart, and F. Rondelez. Dynamics of dewetting. *Physical Review Letters*, 66(6):715–718, 1991.

[21] C. Redon, J. B. Brzoska, and F. Brochard-Wyart. Dewetting and slippage of microscopic polymer films. *Macromolecules*, 27:468–471, 1994.

[22] G. Reiter. Dewetting of thin polymer films. *Physical Review Letters*, 68(1):75–78, 1992.

[23] G. Reiter and R. Khanna. Kinetics of autophobic dewetting of polymer films. *Langmuir*, 16:6351–6357, 2000.

[24] G. Reiter and A. Sharma. Auto-optimization of dewetting rates by rim instabilities in slipping polymer films. *Physical Review Letters*, 80(16), 2001.

[25] G. Reiter, A. Sharma, A. Casoli, M.-O. David, R. Khanna, and P. Auroy. Thin film instability induced by long-range forces. *Langmuir*, 15:2551–2558, 1999.

[26] R. Seemann, S. Herminghaus, and K. Jacobs. Dewetting patterns and molecular forces: A reconciliation. *Physical Review Letters*, 86(24):5534–5537, 2001.

[27] R. Seemann, S. Herminghaus, and K. Jacobs. Gaining control of pattern formation of dewetting films. *Journal of Physics: Condensed Matter*, 13:4925–4938, 2001.

[28] A. Sharma and R. Khanna. Pattern formation in unstabile thin liquid films. *Physical Review Letters*, 81(16):3463–3466, 1998.

[29] A. Sharma and R. Khanna. Pattern formation in unstable thin liquid films under influence of antagonistic short- and long-range forces. *Journal of Chemical Physics*, 110(10):4929–4936, 1999.

[30] A. Sharma and G. Reiter. Instability of thin polymer films on coated substrates: Rupture, dewetting and drop formation. J. Colloid Interface Sci., 178:383–389, 1996.

[31] N. Silvi and E. D. V. On the rewetting of an inclined solid surface by a liquid. *Physics of Fluids*, 28:5–7, 1985.

[32] S. M. Troian, E. Herbolzheimer, S. A. Safran, and J. F. Joanny. Fingering instabilities of driven spreading films. *Europhys. Lett.*, 10(1):25–30, September 1989.

[33] R. Xie, A. Karim, J. F. Douglas, C. C. Han, and R. A. Weiss. Spinodal dewetting of thin polymer films. *Physical Review Letters*, 81(6):1251–1254, 1998.

[34] L. Zhornitskaya and A. L. Bertozzi. Positivity preserving numerical schemes for lubrication-type equations. *SIAM Journal on Numerical Analysis*, 37(2):523–555, 2000.